Oxidation of Metals, Vol. 63, 113-130 (2005) LBNL-55446

Interfacial Segregation, Pore Formation and Scale Adhesion on NiAl Alloys

P. Y. Hou[1] and K. Priimak[1,2]

[1]*Lawrence Berkeley National Laboratory*
Materials Sciences Division
Berkeley, CA 94720

[2]*University of California, Berkeley, CA 94720*

ABSTRACT

Ni-40 and 50at%Al alloys were oxidized at 1000°C for various times in oxygen. Auger electron microscopy was used to study the interface chemistry after scale spallation in ultra high vacuum. The interfacial failure stresses were determined using a tensile pull tester and related to the interface chemistry, pore area and density. Results showed that sulfur started to segregate to areas of the Al_2O_3/Ni40Al interface where the scale was in contact with the alloy after a complete layer of α-Al_2O_3 developed there; the concentration then gradually increased to a steady level of ~2 at%. However, sulfur did not segregate to similar areas of the Al_2O_3/Ni50Al interface even after extended oxidation when it was amply present on interfacial void faces. This behavior demonstrated a strong dependence of interface segregation on NiAl alloy composition. Interfacial failure stress was found to decrease with increasing sulfur content between voids and with higher interface porosity. The level of porosity was strongly related to the sulfur content in the alloy. When Ni40Al was doped with excess sulfur, the segregation behavior did not change, but the interfacial pore density increased significantly. The detrimental effect of sulfur on scale adhesion is two-fold: to weaken the interface and to enhance interfacial pore formation.

KEY WORDS: NiAl, Al_2O_3, oxide/metal interface, segregation, sulfur, adhesion, interface void.

INTRODUCTION

The segregation of indigenous sulfur impurity from an alloy to the Al_2O_3 scale/alloy interface during high temperature oxidation is often considered the major cause that weakens the interface [1-4]. Systematic studies of the chemical changes at Al_2O_3/alloy interfaces as a function of oxidation time have in recent years been carried out for FeCrAl [5], Fe_3Al and FeAl [6,7], where the alloys normally contain about 20 ppm of sulfur. Although sulfur was found to be the major segregant at these scale/alloy interfaces, the segregation behavior, in terms of rate and amount, varied significantly with different alloys and differed from surface segregation. For example, at the Al_2O_3/FeCrAl interface, co-segregation of Cr with S took place, which gave rise to greater than one monolayer of S. The amount saturated as early as 12 minutes at 1000°C, where the rate was determined by S diffusion in the alloy [5,7,8]. For the iron aluminides, S was the sole segregant at these scale/alloy interfaces, but its steady state level was slowly reached only after a complete α-

Al_2O_3 layer formed at the interface [6-8]. On a Fe-40at%Al alloy, this behavior has been shown with conventional as well as field emission Auger electron microscopy [9]. The amount saturated at the intact Al_2O_3/alloy interface was about 0.5 monolayer, but co-segregation of Al and S took place on surfaces of voids that were present at the interface. Whether the same kind of segregation behavior found on FeAl can be expected for NiAl is unknown.

The oxidation behavior of NiAl has been studied extensively [10-18]. The first-formed oxide is θ or γ-Al_2O_3 that grows mainly by cation outward transport [11,15]. α-Al_2O_3 later nucleates at the scale/alloy interface [17] and the initially formed alumina transforms to the more stable α form with time. The α-Al_2O_3 grows by both aluminum outward and oxygen inward transport, with the latter being more dominant [13,15]. Because of this phase transformation, the oxidation kinetics show two parabolic stages separated by a gradual transition. At 1000°C, the rate constant for the initial stage is about 10^{-12} g^2/cm^4s, and it is more than two orders of magnitude faster than the later steady state [12]. Interfacial voids that are several times larger in diameter than the oxide grain sizes are often observed on the alloy surface [10,18-20]. These voids deepen into the alloy with facetted faces and distinct shapes that are associated with the alloy grains. Similar pore formation has been observed on FeAl alloys [21,22]. It was found that most voids nucleated during the initial stage of oxidation [21], where the scale grows predominantly by cation outward transport. Sulfur in the alloy has been suggested to enhance pore formation by lowering its surface energy [23]. Surface impurities can also have the same effect [24].

Despite these prior studies on NiAl, the chemistry of the Al_2O_3/NiAl interface and how it changes with oxidation time have not been systematically examined. The purpose of this work is to study the chemical changes at Al_2O_3/NiAl interfaces as oxidation proceeds, and relates that to the interface morphology and the interfacial strength. The amounts of segregants on interfacial voids (free surface) and on areas where the scale was in contact with the alloy before analysis (interface) are determined separately to compare their segregation behaviors. Preliminary results have been published in a paper [25] that concentrates on the details of the segregation behavior. This paper focuses on the difference between the two compositions of NiAl: Ni-50 and 40 at% Al (both with the β-NiAl structure), and illustrates the relationships between sulfur segregation, interface pore density and interface strength.

EXPERIMENTAL METHODS

Different Ni-50at%Al (NiAl) and Ni-40at%Al alloys were used in this study, all of them made with high purity starting materials. Their compositions and some impurity contents are given in Table 1. Three batches of Ni50Al, identified as NiAl (1-3), and one batch of Ni40Al, identified as Ni40Al(O), were obtained from Oak Ridge National Laboratory. They were prepared by induction melting, followed by annealing at 1300°C for 4 hours. The labels (1)-(3) used to identify the Ni50Al alloys are based on their slightly different S and C contents, where (1) has the lowest levels of both. The purer alloy also

happened to have slightly less Al. One of the Ni40Al alloy, identified as Ni40Al(L), and the S-doped Ni40Al were made at Lawrence Berkeley National Laboratory by arc melting, followed by annealing at 1150°C for 15 hours. All the normal purity alloys contain small amounts of sulfur impurity, about 2-6 ppma. The S-doped alloy was made by co-melting Al and Ni with NiS powders, and it contains more than 30 ppm of sulfur. The oxidation and segregation behaviors are often similar between the three batches of Ni50Al and the two batches of Ni40Al, so unless otherwise noted, the results presented here do not make distinctions between the different batches.

Specimen discs about 1-2 cm in diameter and 1 mm thick were cut from the ingot. All sides of the specimens were grounded using SiC paper with one main face polished to a 1 μm surface finish using diamond paste, and the specimen was cleaned ultrasonically in acetone before oxidation in flowing, dry oxygen. Most oxidation tests were performed at 1000°C, with a few at 1150°C, in a horizontal furnace, where the specimen was placed in an alumina boat with a thermocouple at its back. The assembly was inserted slowly into the hot zone. The specimen surface temperature reached 1000°C in about 10 minutes. After the desired oxidation time, which varied from 10 min to 265 hours, the boat and specimen were quickly pulled out of the furnace and cooled in ambient air. A Cahn TGA system, with a heating rate of 85°C/min, was used for thermogravemetic analysis at 1000°C; both faces of these specimens were polished to a 1 μm finish.

Structure of the scale was studied using X-ray diffraction and the morphology examined using scanning electron microscopy (SEM). Chemistry of the scale/alloy interface was studied using Auger electron spectroscopy (AES) after the scale was removed in the ultra high vacuum (UHV) chamber of the AES by the forces of a scratch made on the specimen surface [26]. This technique caused spalling of the scale adjacent to the scratch, exposing areas of the underlying alloy surface that can be examined using a 0.5-1 μm size Auger probe. The underside of the oxide was also studied on scale pieces that flipped over during the spalling process, so both sides of the interface, although from different locations, can be examined. Images from secondary electrons were used to distinguish features at the alloy surfaces. These usually include smooth facetted void faces or rough Al_2O_3 imprinted interface areas. Several different areas covering more than one alloy grains were examined. Surveys were performed on many similar features in order to obtain a statistical analysis of the results.

The strength of the scale/alloy interface was determined using a Quad Group Sebastian 5 tensile-tester, where a 3 mm diameter stud with a thin film of adhesive was bonded onto the oxidized surface. The stud was then pulled at an inverted position (Fig. 1a) with a constant loading rate until failure occurs, which was always abrupt. If failure took place at the scale/alloy interface, an example is shown in Fig. 1b, and if more than 75% of the interfacial area was exposed, the data was considered useful and the interface strength was determined by dividing the failure load over the entire stud area. The adhesive was cured at 150°C for 1 hr and has a maximum strength of 103 MPa. Three or four studs were tested on each specimen, and every failed area was subsequently examined under the SEM.

Quantification of interfacial pores was made by analyzing SEM micrographs of the exposed alloy surface. Images magnified 2000 times were randomly taken within the pulled areas, covering several different alloy grains. Only pores greater than the imprints made by α-Al_2O_3 oxide grains can be unambiguously identified. Therefore, pores that were counted had a minimum diameter of about 0.5 μm. Analysis was done using Image Pro Plus software, either by manually defining the perimeter of a pore to get the pore face area that lays at the scale/alloy interface, or a simple count of the number of pores.

RESULTS

Specimen weight gain as a function of time was examined for all the alloys at 1000°C up to 50 hours. All results showed a fast initial stage followed by a slower steady state; the rates of both stages obeyed parabolic kinetics and the rate constants for the two stages are in the range of $(2\text{-}6)\times10^{-12}$ and $(2\text{-}5)\times10^{-14}$ g^2/cm^4s respectively. These numbers agree well with those reported by others for NiAl [14]. XRD studies indicated that the early stage scales on both Ni50Al and Ni40Al were θ-Al_2O_3; α-Al_2O_3 developed later and it nucleated at the scale/alloy interface. Typical oxide morphology after a layer of α-Al_2O_3 formed at the interface is shown in Fig. 2. Under the current oxidation condition, this Al_2O_3 phase transformation process barely started at 5hrs on the Ni50Al, but the entire Ni40Al interface was covered with α-Al_2O_3 by 3hrs, indicating slower transformation on alloys with higher Al contents. After scale removal, α-Al_2O_3 grain imprints are clearly seen on the alloy side of the interface; an example is given in Fig. 3(b). Prior to the development of this α-Al_2O_3 layer at the interface, the alloy was in contact with fined-grained θ-Al_2O_3, and this morphology is shown in Fig. 3(a).

Large and easily distinguishable voids were often found on the alloy surface after scale removal (Figs. 3a and 4). As with FeAl [21], they developed early, were highly facetted with their shapes dictated by the alloy grain orientation, grew in size and coalescenced with oxidation time. The number density was significantly lower on Ni50Al (averaging less than $0.3\times10^{-2}/\mu m^2$) than Ni40Al ($>1\times10^{-2}/\mu m^2$), but the pore sizes on both alloys were similar for a given oxidation time. Addition of sulfur to the Ni40Al alloy resulted in a much greater density of voids at the interface; a comparison is shown in Fig. 4. Number density as high as $0.1/\mu m^2$ was found on the specimen oxidized for only 30 minutes.

No impurities were detected on the oxide side of the interface; only O and Al were observed. All impurities, if present at the interface, remained on the alloy side after scale removal in UHV. The chemistry found on void faces served as a direct comparison of segregation behaviors between free surfaces and oxide/alloy interfaces. Figure 5 summarizes the change of sulfur content on interfaces and void surfaces on Ni-40 and -50Al. Most oxidations were performed at 1000°C. A few were carried out at 1150°C (3 and 100 hrs) and each one was plotted against an 'equivalent time' at 1000°C. This is the time necessary to produce the same scale thickness as that at 1150°C, and it was

determined using the oxidation rates of the two temperatures, assuming the scale to be fully dense α-Al_2O_3.

The most surprising result from Fig. 5 is that S segregated to the interfaces of Al_2O_3/Ni40Al, but not to Al_2O_3/Ni50Al. The latter sometimes contain small amounts of B and/or P [25,8], but S was never detected. A typical AES spectrum from this S-free interface is shown in Fig 6(c). On the Ni40Al, sulfur was the only impurity found; an example is given in Fig. 6b. Similar to Fe40Al [9], S only segregated to the interface after a complete α-Al_2O_3 layer developed there, which at 1000°C was about 3 hrs. Its subsequent buildup at the interface was gradual, reaching a stead-state level after longer oxidation times to 2 at%, which is equivalent to about 0.2 monolayer. The two batches of Ni40Al, made at ORNL or LBNL, behaved similarly. At the higher temperature of 1150°C, the amount of S at the interface was comparable to that found at 1000°C. Interface composition for the S-doped samples is absent from Fig. 5 due to the presence of numerous tiny voids on the S-doped Ni40Al. These voids are much smaller than the Auger probe size, and they were not resolvable under the SEM of the scanning Auger. Analysis on what appears to be an interface area could therefore include one or more of these voids and give erroneous results of the chemistry of a true interface.

On the void faces of Ni50Al, carbon was first found, then later replaced by sulfur [25]. As seen in Fig. 5, S on Ni50Al voids was only observed after 100 hrs at 1000°C. The coverage on Ni40Al void faces, on the other hand, was much faster, even though the two types of alloys contain similar amounts of sulfur in the bulk (Table 1). Various levels of S were detected on different void faces. This variation was associated with different shapes of voids that were present on different alloy grains, which indicates some degree of orientation dependent S segregation on NiAl surfaces. Within the error bars, about three levels, 2, 5 and 7 at%, were found on the void faces of Ni50Al. On Ni40Al, the levels ranged from 5, 7, 9-10 to 12 at%; an AES spectrum from a 7 at% void face on Ni40Al is given in Fig. 6(a). The 3% found on the normal purity Ni40Al after only 10 min oxidation is likely the result of an unsaturated surface, where saturation is limited by the S concentration and its diffusion rate in the alloy. The S-doped Ni-40Al, containing >30 ppm S, showed similar segregation behavior as the normal purity Ni-40Al that contains only a few ppm of S, but saturation was reached much earlier, as expected.

The relationship between interfacial failure stress and interface sulfur concentration is shown in Fig. 7a. The failure strength was obtained by averaging 3-4 pull test results from a single sample, and this strength is plotted against the average sulfur content found on the same specimen, as determined by AES after scratching. Specimens were oxidized at 1000°C for times between 26-100 hrs for the Ni50Al and 3-100 hrs for the Ni40Al. All samples had the same interface morphology of α-Al_2O_3 imprints and occasional voids. The failure strength is seen to drop quickly with interface S content, but only for the Ni40Al where S was detected. Ni50Al alloys that did not have any S at the interface also showed a range of failure strengths between 30-90 MPa. This scatter was not related to interface chemistry, such as the occasional presence of P and/or B, even though B is known to strengthen alloy grain boundaries [27]. The fact that all S-free Al_2O_3/Ni50Al interfaces failed at a range of strengths suggests that there were other factors contributing to scale

adhesion. Interface porosity, which increased with oxidation time (as seen in Fig. 7b), and being crack-like defects, should be the most likely candidates.

Although the trend in Fig. 7a for Ni40Al indicates a strong interface weakening effect by the presence of sulfur, it should be noted that the variation in sulfur content was obtained from specimens oxidized at different times, so these samples have different scale thickness. Although the pull test results are not sensitive to film thickness, longer oxidation times can cause more defects in the scale and at the interface. Figure 7b shows the interface porosity of each of the Ni40Al specimen whose sulfur content was presented in Fig. 7a. Specimens that had more sulfur at the interface also had greater interfacial porosity; both related to longer oxidation times.

Figure 8 compares the fracture strength as a function of interface pore density. In this plot, each strength data point was obtained from one pull stud. The number of pores at the exposed interface under that particular stud was calculated from several randomly taken SEM micrographs and plotted against the strength. To avoid different pore sizes from different oxidation conditions, all the data points were from specimens oxidized at 1000°C for 26 hours. Since the pore size on these alloys under a given oxidation condition was similar, the pore density can be used to give a good indication of the extent of defect concentration. The S-doped Ni40Al was not included, because all of its scale spalled upon cooling such that no pull tests could be performed. Results in Fig. 8 show a quick drop in interface strength with increasing pore density. However, the data seem to fit two different lines, with one (the dashed line) having a slower decreasing rate and a higher strength for a given pore density. This line runs through data points from Ni50Al whose interface was S-free, but had a rougher, 240 grit SiC finished starting surface, i.e., those identified as Ni50Al(3)r. This rougher surface gave rise to higher interfacial pore density; the same phenomenon had been observed on Fe40Al [24].

For all the normal 1μm diamond surface finish, the number of pores on Ni40Al is seen to be higher than that on Ni50Al, and this number could vary quite a bit even within one sample (see for example, the three data points from the Ni40Al(L) specimen). This shows that pore distribution is not uniform, similar to what was observed on Fe40Al [21]. The highest purity Ni50Al (batch 1) did not show interfacial failure after 26 hrs. That is why its data are not present on this figure. Quantification of pore developments on these alloys, which will be presented in a later paper [28], shows that the purity level of these alloys significantly influence interfacial pore formation. Pore formation is also related to the stoichiometry of the NiAl alloy, as previously reported by Blumm and Grabke [18].

When the fracture strength is compared with the interface pore area instead of the pore density (Fig. 9), the data became more scattered due to variations in pore size as well as density throughout the interface on every specimen. Figure 9 includes data from specimens oxidized at 1000°C after 26-100 hrs. The times were 50 and 65 hrs for Ni50Al(1), 26 and 100 hrs for Ni50Al(2), 50 hrs for Ni50Al(3), 26 hrs for Ni50Al(3)r, 26 and 50 hrs for Ni40Al(O) and 26, 50 and 100 hrs for Ni40Al(L). On every alloy, it was found that the pore fraction increased with longer oxidation time. Within the scatter, the beneficial effect of S-free interfaces of the Ni50Al alloy is still obvious (as indicated by the

dash line). Under the same specimen surface finish, the Ni40Al alloys again developed greater total porosity than the Ni50Al alloys. Strength dropped very quickly with increasing pore fraction at the interface, then leveled off to a constant value. This level may no longer be dominated by the interface strength, but may be dictated by oxide fracture.

DISCUSSIONS

The segregation behavior at Al_2O_3/Ni50Al and Ni40Al interfaces showed some interesting phenomena. First of all, S did not segregate to Al_2O_3/Ni50Al interfaces even after 265 hrs at 1000°C or 100 hrs at 1150°C, when S already covered the void faces that were present at the interface. Of all the Al_2O_3-forming alloys studied by this method, i.e., AES after in-situ scratching [8], this is the first alloy where segregation to the interface did not occur. On the other hand, the slightly Ni-rich alloy, namely Ni40Al, which has the same phase and similar bulk impurity contents as the Ni50Al, forming an interface with the same type of oxide under the same oxidation conditions, consistently showed sulfur at its interface after a complete α-Al_2O_3 developed, reaching a level of about 2 at%. This behavior is similar to that previously observed on Fe-40Al [9].

Why should sulfur segregate to one Al_2O_3/NiAl interface but not the other, simply because of a difference in alloy composition? A possible explanation may lie in the relative stability of the two Al_2O_3/NiAl interfaces. It is known that the ordered Ni50Al has a lower surface energy than Ni40Al [29]. Limited surface segregation study has shown that more S segregated to a Ni50Al single crystal surface when the surface was enriched with Ni from preferential sputtering of Al [30]. There is no prior information on the interface energy or the interface segregation behavior of the two alloys. However, indirect evidence from wetting studies of NiAl on sapphire shows that the Al_2O_3/NiAl interface energy decreases with increasing Al content in NiAl [31]. Theoretical analysis on metal/ceramic bonding have also shown that the interface energy between Ni(Al)/Al_2O_3 decreases with increasing Al activity near the alumina dissociation P_{O2} [32]. These studies suggest that the Al_2O_3/Ni40Al interface formed during oxidation would have a higher energy than that of the Al_2O_3/Ni50Al. In that case, sulfur segregation should be more favored on the former to lower its energy.

The diffusion of S in Ni50Al must be significantly slower than in Ni40Al, since interfacial voids on Ni50Al were not covered with S until after oxidation times greater than 100 hrs at 1000°C. Yet for the same amount of bulk S in Ni40Al (2-6 ppm), these void faces were covered with S as early as 0.5 hrs at 1000°C. Using the model of Lea and Seah [33], diffusion coefficients of S in the two alloys at 1000°C are calculated to be about 1.6×10^{-7} cm^2/s for Ni40Al and 1×10^{-9} cm^2/s for NiAl. Diffusion of Ni in NiAl is known to be very sensitive to stoichiometry [34] due to strong variations of defect concentrations with composition. At 1300K, D_{Ni} increases from 10^{-12} to 10^{-11} cm^2/s from stoichiometric NiAl to Ni-40at%Al. These values are 10^3 to 10^4 times lower than the D_S calculated from the current segregation results, and the effect of composition on S diffusion seems to be stronger than that on Ni. The 10^3-10^4 difference in diffusivity between S and Ni agrees

with recent data from S segregation studies on Ni50Al surfaces [30], which determined that S diffusion in Ni50Al was about 3 orders of magnitude faster than Ni at 800°C. On both alloys, the amount of segregated S was found to depend on void face orientation. Work is in progress to determine the orientation of different void faces using electron backscatter diffraction (EBSD), in order to correlate the segregation behavior to crystallography.

Considerably more voids were found on Ni40Al than Ni50Al, similar to results reported by Brumm and Grabke [18]. Nucleation of voids seems to be much easier on Ni40Al than on Ni50Al, giving rise to higher pore density at the interface. The greatest effect of excess sulfur in Ni40Al was to increase the number of interfacial voids. The void density after only 30 min at 1000°C was as high as $0.1/\mu m^2$, while the average number density on the regular purity Ni40Al (from 5-100 hr oxidation at 1000°C) was only $0.01/\mu m^2$. Since the energy barrier for heterogeneous nucleation of a void is proportional to $(2+\cos\theta)(1-\cos\theta)^4 \gamma_m^3 / \Delta G_v^3$ [35], where ΔG_v is the volume free energy change of void nucleation, γ_m the surface energy of the metal and θ the angle between the pore edge and the oxide scale. Segregation of S to the initial void embryo would reduce γ_m, and θ as well if the interface and oxide surface energies remain the same. This reduction of the nucleation energy barrier can explain why more voids formed on the S-doped Ni40Al, as similar effects were found on Fe40Al with impurity doping on the alloy surface prior to oxidation [24]. The same reasoning, however, cannot explain the difference in pore nucleation tendencies between the two NiAl alloys. Since γ_m of Ni40Al is higher than that of Ni50Al [29], void nucleation should be harder for the former, but experimental results show the opposite. In this case, pore nucleation may be dominated by the higher number of point defects in Ni40Al [36] and/or their greater mobility [37].

The pull test used in this study is a technique that lacks a well-defined pre-crack so that failure depends on internal defects of unknown size and location. Stress concentration will also be higher at the stud edges, although this problem is alleviated by the spreading of some of the adhesive around the edge. The technique has the advantage that it is not as sensitive as other commonly used methods to the mechanical properties of the oxide or the alloy or to the scale thickness; it is also easy and has been used on many other scale/alloy systems [38]. When failures occur at the interface, the fracture strength gives an indication of the stress at which the scale is separated from the alloy. Defects that are present at the interface can act as crack initiators. Although the technique is inherently stochastic, a statistical analysis of the failure stresses directly correlated to interface defect concentration and chemistry can still be useful in providing a trend that shows relationships between failure and interface property.

The results of Figs. 7-9 show that Al_2O_3 scale adhesion on NiAl is related to the degree of interfacial porosity as well as the interface sulfur content. The dependence on porosity is not surprising, since the failure stress σ, is proportional to $K_{IC}/\sqrt{\pi c}$, where K_{IC} is the interfacial fracture toughness and c the critical defect size. Higher pore density and larger pore area fraction give rise to greater effective c. The more difficult question is the relative importance of defects and chemistry on interfacial strength. The fact that interfacial S and porosity both increase with oxidation time (Fig. 7b) makes it even harder

to separate the two. However, by introducing more interface porosity through an initially rough polished surface, the strength of S-free and S-containing interface with similar pore density can be compared (Figs. 8,9). Although data scattering was large due to the random nature of pore formation, results show that under the same porosity, interfaces that contain sulfur was weaker. This could arise from a reduced interfacial toughness, where S at areas between pores weakens the interface to allow easier crack propagation.

Excess sulfur in Ni40Al greatly increased the number of interfacial pores, which is believed to be the reason why these scales were extremely non-adherent and spalled easily upon cooling. The amount of S segregated at the interface is probably not different from that found on the low sulfur Ni40Al. Although due to the presence of many sub micro-sized voids, conventional AES using a 0.5-1 μm probe cannot clearly identify true interface areas, the amount of S segregated on large void surfaces did not vary with alloy S content. The same, therefore, is expected for the interface.

CONCLUSIONS

- Sulfur impurity in Ni50Al (2-5 ppm) did not segregate to Al_2O_3/Ni50Al interfaces where the scale was in contact with the alloy, but the same level in Ni40Al segregated after a complete α-Al_2O_3 layer formed at the interface.
- Based on the rate of sulfur segregation to internal void surfaces, S diffusion in Ni50Al and Ni40Al at 1000°C was calculated to be approximately 1×10^{-9} and 1.6×10^{-7} cm^2/s respectively. Segregation on void faces showed dependence on crystallographic orientation.
- Ni40Al had higher numbers of interfacial voids compared to Ni50Al. Doping the Ni40Al with excess sulfur significantly increased the interfacial void density.
- The fracture strength of these interfaces decreased with increasing interfacial porosity. Under the same degree of porosity, sulfur-free interfaces were stronger than S-containing ones.
- The role of sulfur on scale adhesion is two-fold: to enhance pore formation by lowering its nucleation energy, and to weaken the interface by accelerating crack propagation between pores.

ACKNOWLEDGMENT

The author would like to thank Dr. Bruce Pint of ORNL for supplying some of the alloys. This research is sponsored by the U. S. Department of Energy under contract No. DE-AC03-76SF00098.

REFERENCES

1. Y. Ikeda, K. Nii and K. Yoshihara, *Trans. Japan Inst. Met. Suppl.*, **24**, 207 (1983).
2. A. W. Funkenbusch, J. G. Smeggil, and N. S. Bornstein, *Metall. Trans. A*, **16A**, 1164 (1985).
3. D. Lees, *Oxid. Met.*, **27**, 75 (1987).
4. J. L. Smialek, *Metall. Trans.* **22A**, 739 (1991).
5. P. Y. Hou, *Mater. and Corr.*, **51**, 329 (2000).
6. P. Y. Hou, "Sulfur Segregation to Growing Al_2O_3/alloy Interfaces", *J. Mater. Sci. Lett.*, **19**, 577-8 (2000).
7. P. Y. Hou, *Mater. Sci. Forum*, **369-372**, 23 (2001).
8. P. Y. Hou, "Segregation Phenomena at Growing Alumina/Alloy Interfaces", *J. Corr. Sci. Eng.*, **6**, paper 75 (2003).
9. P. Y. Hou and John Moskito, "Sulfur Distribution on Al_2O_3/FeAl Interfaces Studied by Field Emission-Auger Electron Spectroscopy", *Oxidation of Metals* **59**, 559-574 (2003).
10. R. Hutchings, M. H. Loretto and R. E. Smallman, *Metal Science*, **15**, 7 (1981).
11. E. W. A. Young and J. H. W. de Wit, *Solid State Ionics*, **16**, 39 (1985).
12. J. Doychak and M. Rühle, *Oxid. Met.*, **31**, 431 (1989).
13. B. A. Pint, J. R. Martin and L. W. Hobbs, *Oxid. Metals*, **39**, 167 (1993).
14. M. W. Brumm and H. J. Grabke, *Corr. Sci.*, **33**, 1677 (1992).
15. R. Prescott, D. F. Mitchell and M. J. Graham, *Corrosion*, **50**, 62 (1994).
16. E. Schumann J. C. Yang, M. J. Graham and M. Rühle, *Mater. Corros.*, **46**, 218 (1995).
17. J. C. Yang, K. Nadarzinski, E. Schumann and M. Rühle, *Scripta Met*, **33**, 1043 (1995).
18. M. W. Brumm and H. J. Grabke, *Corros. Sci.*, **34**, 547 (1993).
19. J. L. Smialek, *Met. Tran. A*, **9A**, 309 (1978).
20. H. M. Hindam, and W. W. Smeltzer, *J. Electrochem. Soc.*, **127**, 1630 (1980).
21. P. Y. Hou, Y. Niu and C. Van Lienden, *Oxid. Met.*, **59**, 41 (2003).
22. C. H. Xu, W. Gao and H. Gong, *High Temp. Mater. and Proc.*, **19**, 371 (2000).
23. H. J. Grabke, D. Wiemer and H. Viefhaus, *Appl. Surf. Sci.*, **47**, 243 (1991).
24. P. Y. Hou and C. Van Lienden, *Mater. High Temp.* **20**, 357 (2003).
25. P. Y. Hou, "Chemical and Morphological Changes at Al_2O_3/NiAl Interfaces and Their Relationship to Scale Adhesion", in "*High Temperature Corrosion and Materials Chemistry, IV*," eds. E. Opila, P. Hou, T. Maruyama, B. Pieraggi, M. McNallan, D. Shifler, and E. Wuchina, the Electrochemical Society, PV 2003-16, pp. 40-50, 2003.
26. P. Y. Hou, in *"High Temperature Corrosion and Materials Chemistry"*, ed. P. Y. Hou, M. J. McNallan, R. Oltra, E. J. Opila and D. A. Shores, pp. 198-210, the Electrochem. Soc., 1998.
27. C. T. Liu, E. H. Lee, E. P George and A. J. Duncan, "Intergranular fracture tendency in NiAl doped with boron and carbon," *Scripta Met*, **30**, 387-92 (1994).
28. K. Priima and P. Y. Hou, "A comparison of pore formation at the interfaces between Al_2O_3 and NiAl, S-doped NiAl, FeAl and NiPtAl," manuscript in preparation.
29. G. D. Ayushina, E. S. Levin, P. V. Del'd, *Russ J. Phys. Chem.* **43**, 2756 (1969).
30. L. Rivoaland, V. Maurice, P. Josso, M.-P. Bacos and P. Marcus, "The effect of sulfur segregation on the adherence of the thermally-grown oxide on NiAl – I. sulfur segregation on the metallic surfaces of NiAl(001) single crystals and at NiAl(001)/Al_2O_3 interfaces", *Oxid. Metals*, **60**, 137-158 (2003).
31. E. Saiz, R. M. Cannon and A. P. Tomsia, "Reactive spreading: adsorption, ridging and compound formation," *Acta mater.*, **48**, 4449-4462, 2000.
32. W. Zhang, J. R. Smith and A. G. Evans, 'The connection between *ab initio* calculations and interface adhesion measurements on metal/oxide systems: Ni/Al_2O_3 and Cu/Al_2O_3', *Acta Mater.*, **50**, 3803-3816 (2002).

33. C. Lea and M. P. Seah, *Philo. Mag.*, **35**, 213 (1977).
34. St. Frank, S. V. Divinski, U. Sodervall and Chr. Herzig, *Acta mater.*, **49**, 1399 (2001).
35. D. P. Woodruff, *The Solid-Liquid Interface*, Cambridge University Press, p. 21-38, 1973.
36. S. M. Kim, Y. Takeda and M. Kogachi, "Observation of high temperature Al vacancies and Al antistructure atoms in B2 NiAl alloys by in situ neutron diffraction", *Scripta Materialia*, **34**, 1845-50, 1996.
37. Bai Bin, Fan Jiawen and G. S. Collins, "Vacancy mobility in nickel aluminide versus composition", in *Diffusion Mechanisms in Crystalline Materials*, ed. Y. Mishin, G. Vogl, N. Cowern, R. Catlow and D. Farkas, MRS Proceeding, pp.203-8, 1998, Mater. Research Soc., Warrendale, PA, USA.
38. P. Y. Hou and S. Saunders, "A Survey of Test Methods for Scale Adhesion Measurement," Workshop on scale growth and exfoliation in steam plant, Sept. 3-5, 2003, National Physical Laboratory, Teddington, UK, to be published in *Mater. High Temp.*

FIGURE CAPTIONS

Figure 1: (a) Schematics of the pull test setup, (b) example of a failed area on Ni40Al after oxidation at 1000°C for 26h.

Figure 2: SEM image of a piece of scale from Ni40Al oxidized at 1000°C for 5 hrs showing a two-layered morphology. The surface layer consists of needle shaped grains typical of the first-formed transition alumina. The underside contains a layer of α-Al_2O_3 that nucleated later at the scale/alloy interface.

Figure 3: SEM micrographs of Ni40Al surfaces after scale removal. The alloy was oxidized at 1000°C for (a) 10 min and (b) 3 hrs.

Figure 4: Comparison of pore density on (a) normal purity Ni40Al, and (b) S-doped Ni40Al after oxidation at 1000°C for 30 minutes. The white color void faces have a layer of oxide film on them due to scale cracking and oxygen ingress during cooling.

Figure 5: The buildup of sulfur with oxidation time at Al_2O_3/alloy interfaces and interfacial void surfaces of Ni40Al and Ni50Al. Specimens oxidized at 1150°C were plotted against times necessary to develop the same scale thickness at 1000°C.

Figure 6: Typical AES spectra of void surface, Ni40Al and Ni50Al Interfaces. (a) Void surface on Ni40Al(L) after 26 hr, (b) interface of Ni40Al(L) after 26 hrs and (c) interface of Ni50Al(2) after 100hrs.

Figure 7: Relationships between interface sulfur content and (a) interfacial fracture strength, and (b) interface porosity. Numbers next to data points represent the oxidation time in hours.

Figure 8: Relationship between interfacial failure stress and interface pore density. All specimens were oxidized at 1000°C for 26 hr. The Ni50Al(3)r had a surface finish on 240 grit SiC; all other specimens were finished on 1 μm diamond.

Figure 9: Relationship between interfacial strength and interface pore area. Data include oxidation times ranging from 26-100 hrs at 1000°C.

Table I: Compositions of the alloys determined by GDMS or ICP-OE analyses.

Alloy	Concentration (at%)		Concentration (ppma)				
	Ni	**Al**	**S**	**C**	**Cl**	**P**	**B**
NiAl (1)	50.7	49.3	3.5*	320	<0.01*	2.8*	43.8*
NiAl (2)	49.91	50.05	3.7*	360			40
NiAl (3)	49.74	50.19	4.3*	710			
Ni40Al (O)	59.7	40.3	6.6*	380			30
Ni40Al (L)$^{+}$	60.1	39.8	2.2*	150			
Ni-40Al (S-doped)$^{+}$	60.9	40.0	34.7*	420			

$^{+}$Alloys made at LBL. Others were made at ORNL.

*From GDMS (glow discharge mass spectroscopy) analysis, others were obtained using ICP-OE (inductively coupled plasma spectrometer-optical emission) analysis.

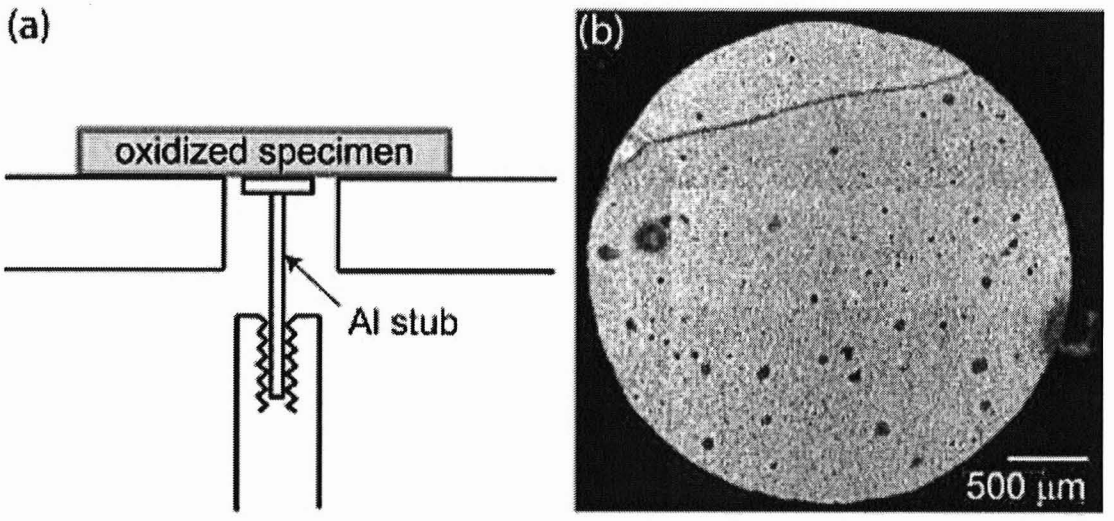

Figure 1:(a) Schematics of the pull test setup, (b) example of a failed area on Ni40Al after oxidation at 1000oC for 26h.

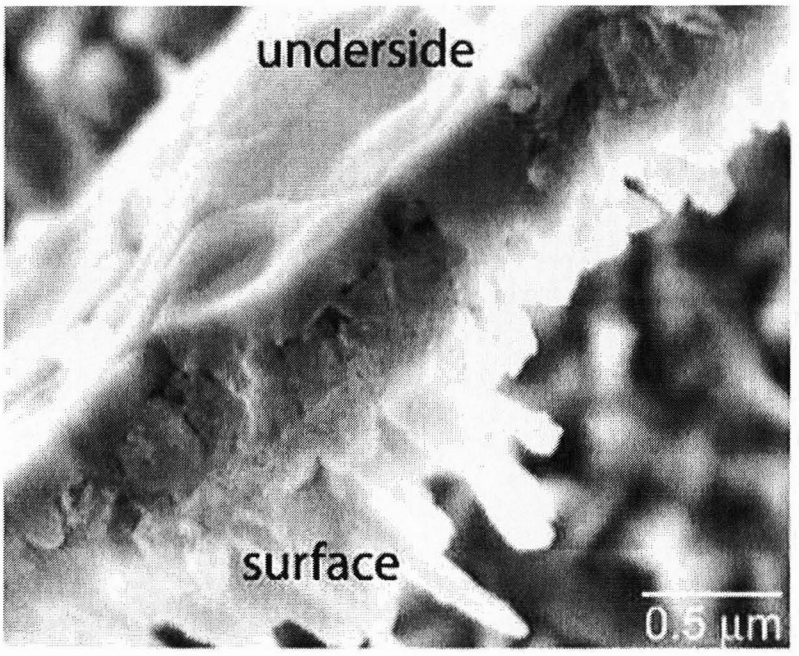

Figure 2: SEM image of a piece of scale from Ni40Al oxidized at 1000oC for 5 hrs showing a two-layered morphology. The surface layer consists of needle shaped grains typical of the first-formed transition alumina. The underside contains a layer of -Al2O3 that nucleated later at the scale/alloy interface.

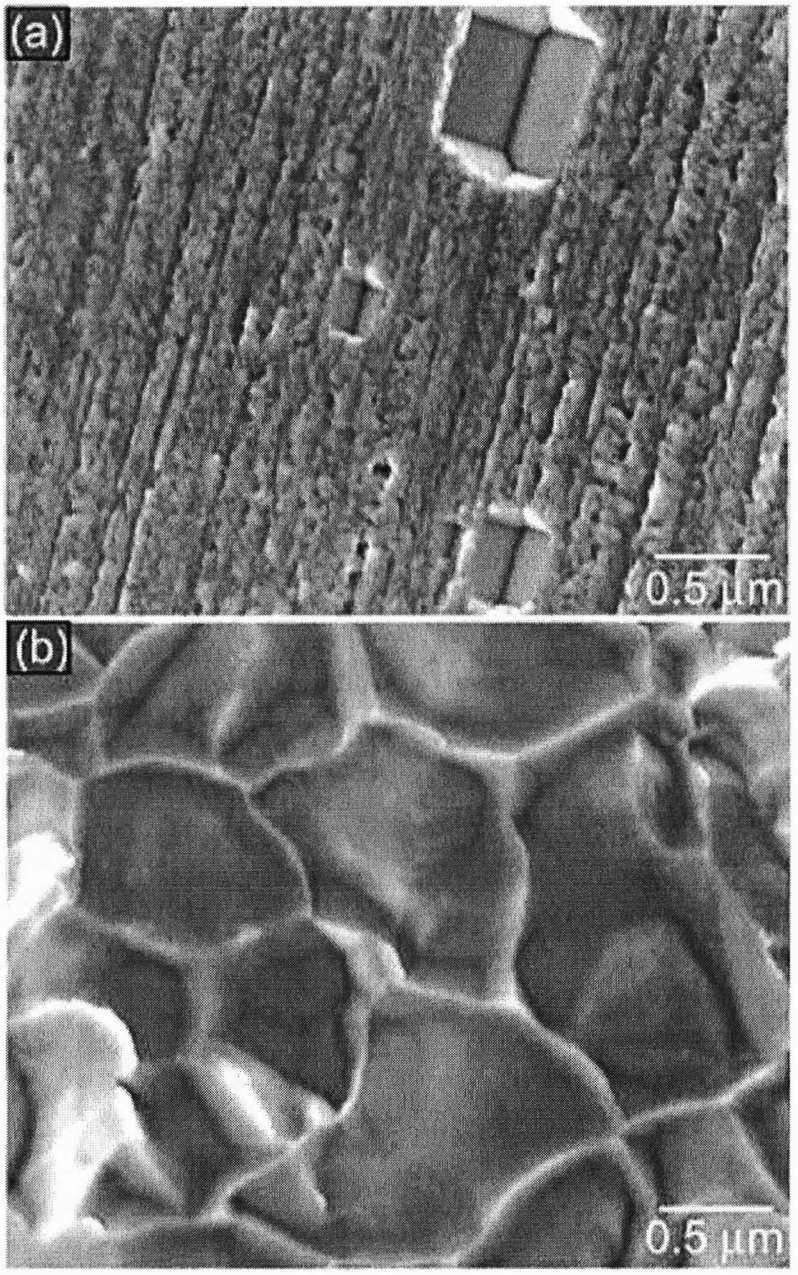

Figure 3: SEM micrographs of Ni40Al surfaces after scale removal. The alloy was oxidized at 1000oC for (a) 10 min and (b) 3 hrs.

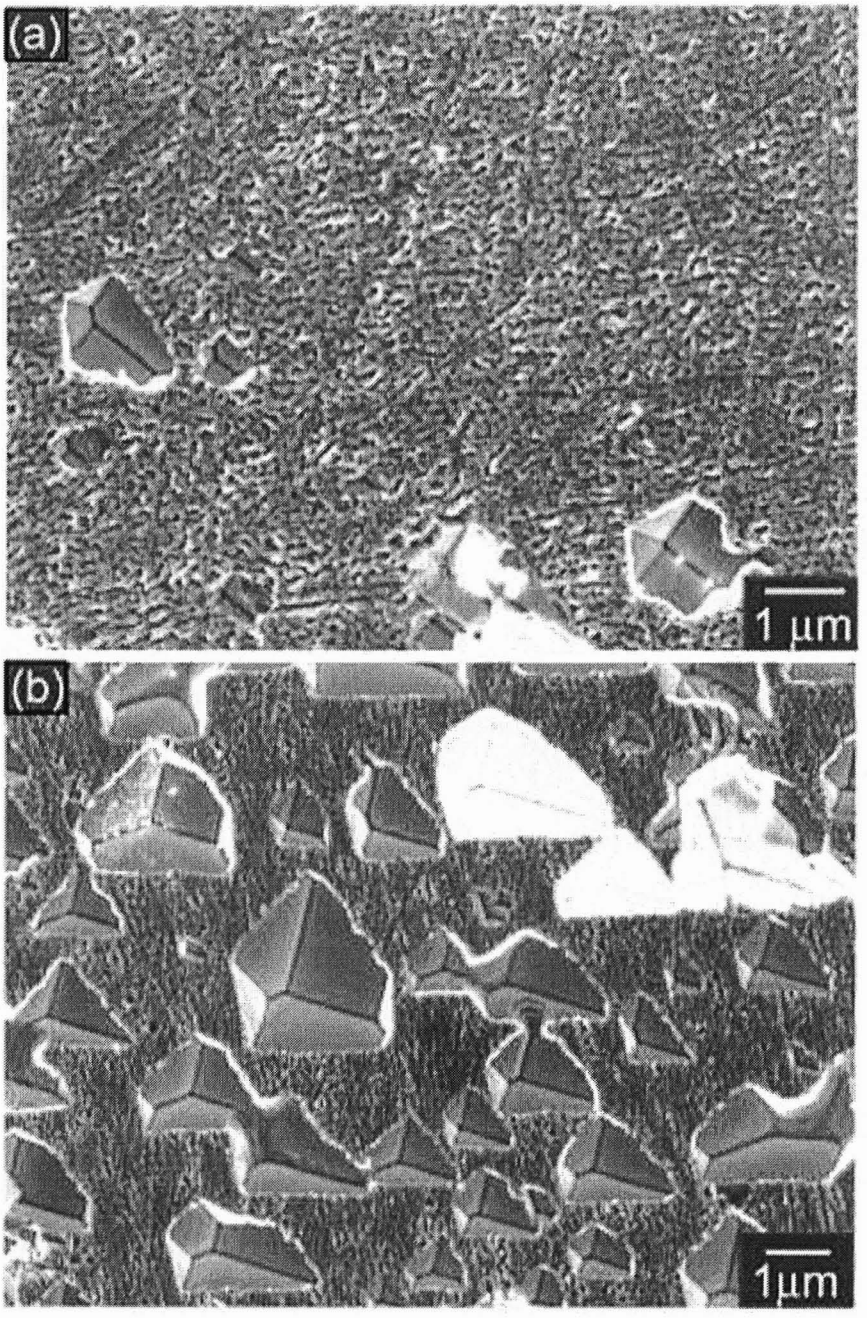

Figure 4: Comparison of pore density on (a) normal purity Ni40Al, and (b) S-doped Ni40Al after oxidation at 1000oC for 30 minutes. The white color void faces have a layer of oxide film on them due to scale cracking and oxygen ingress during cooling.

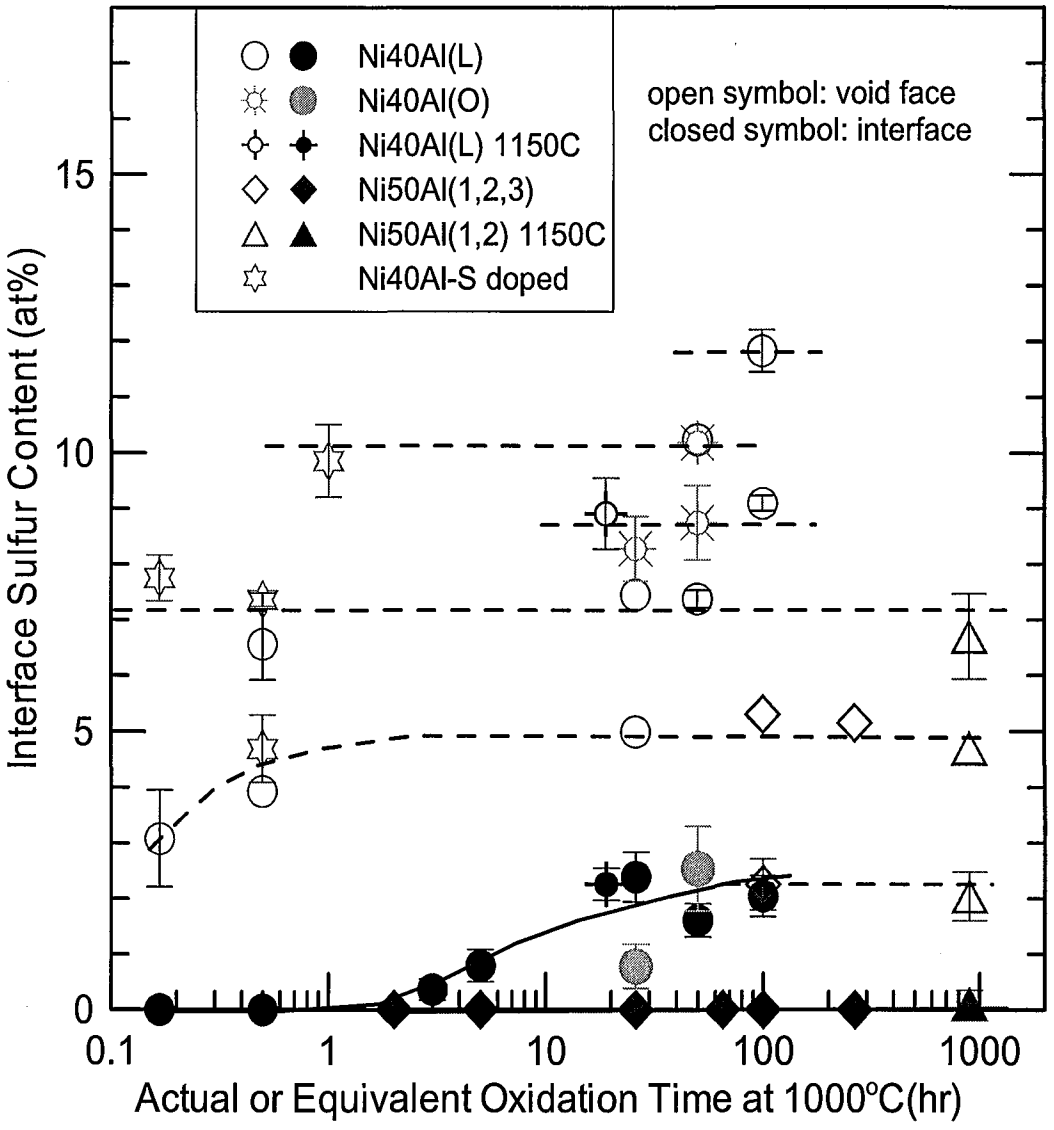

Figure 5: The buildup of sulfur with oxidation time at Al_2O_3/alloy interfaces and interfacial void surfaces of Ni40Al and Ni50Al. Specimens oxidized at 1150oC were plotted against times necessary to develop the same scale thickness at 1000°C.

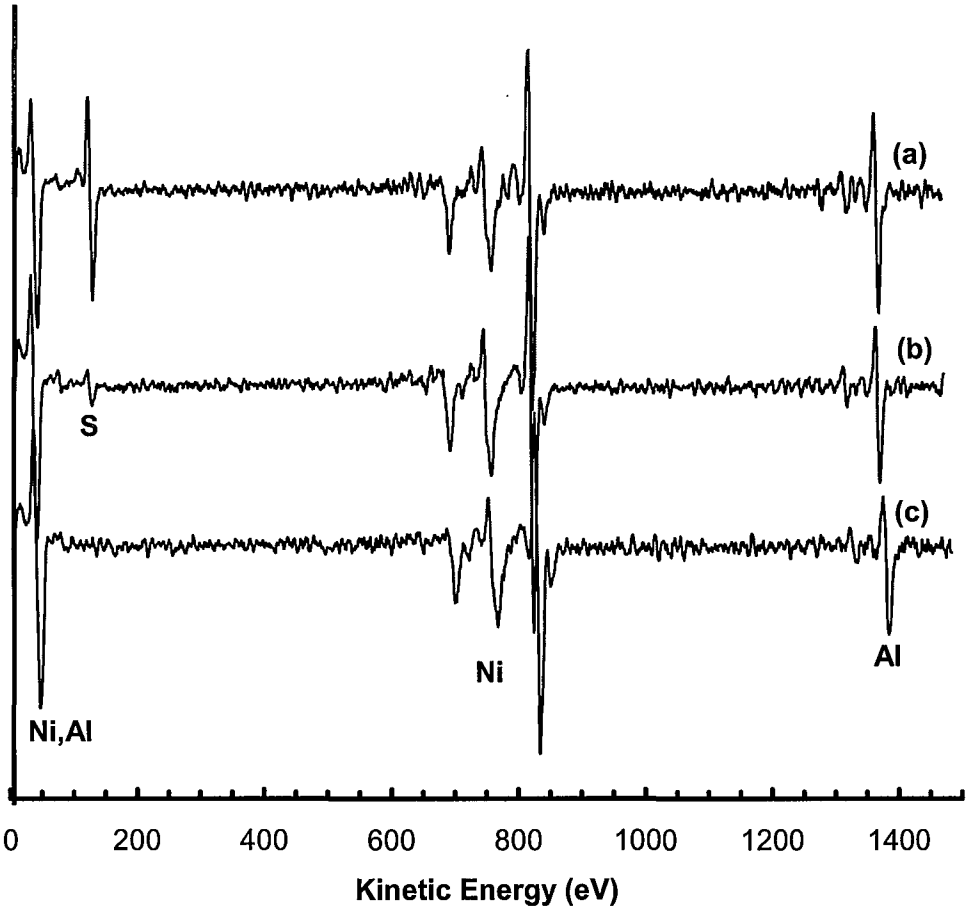

Figure 6: Typical AES spectra of void surface, Ni40Al and Ni50Al Interfaces. (a) Void surface on Ni40Al(L) after 26 hr, (b) interface of Ni40Al(L) after 26 hrs and (c) interface of Ni50Al(2) after 100hrs.

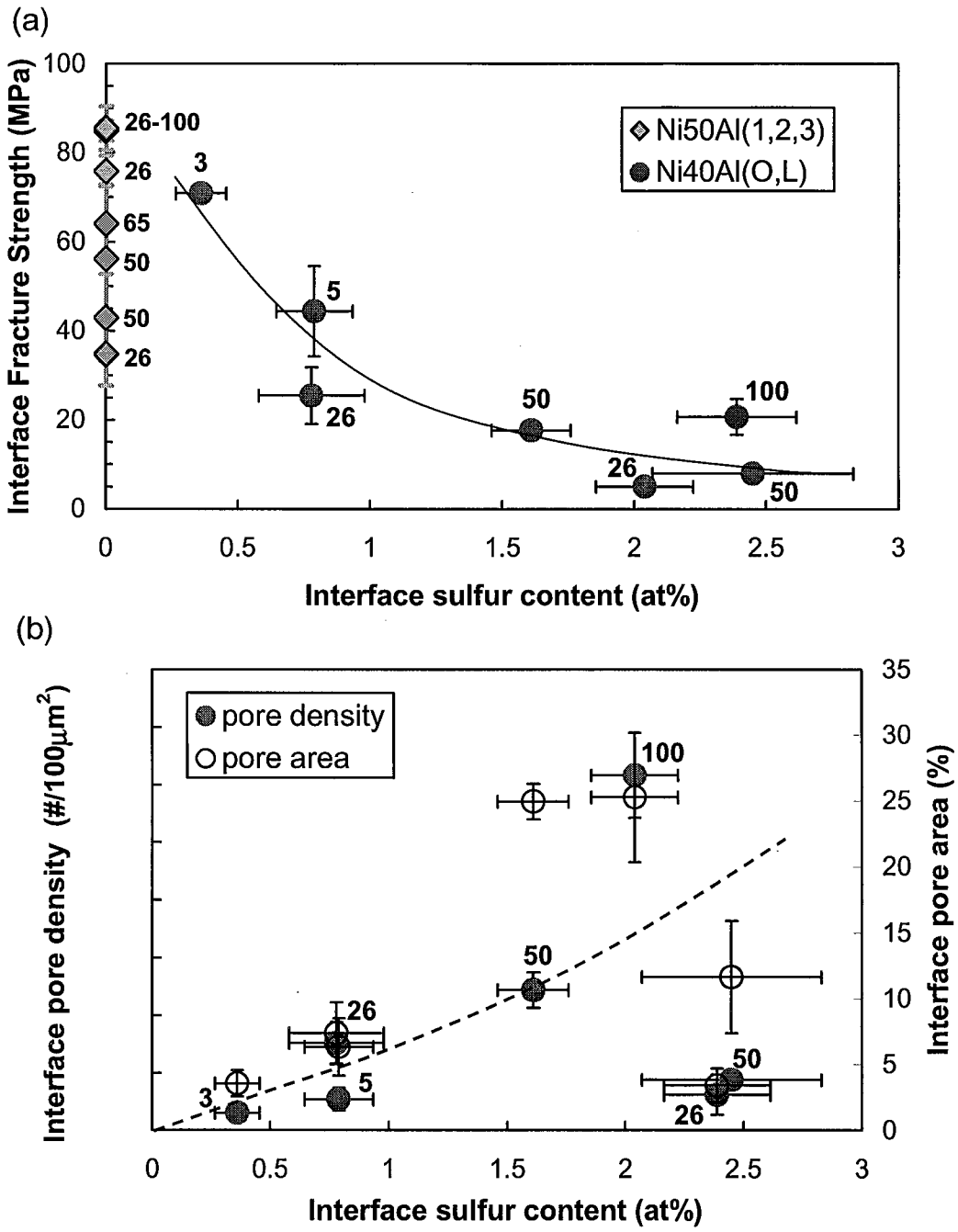

Figure 7: Relationships between interface sulfur content and (a) interfacial fracture strength, and (b) interface porosity. Numbers next to data points represent the oxidation time in hours.

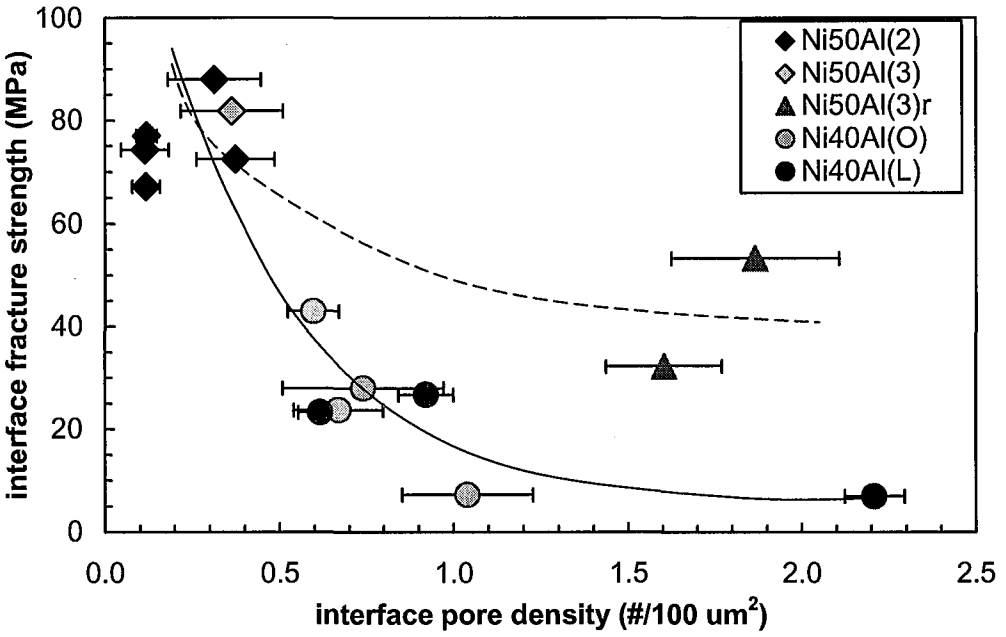

Figure 8: Relationship between interfacial failure stress and interface pore density. All specimens were oxidized at 1000°C for 26 hr. The Ni50Al(3)r had a surface finish on 240 girt SiC; all other specimens were finished on 1 μm diamond.

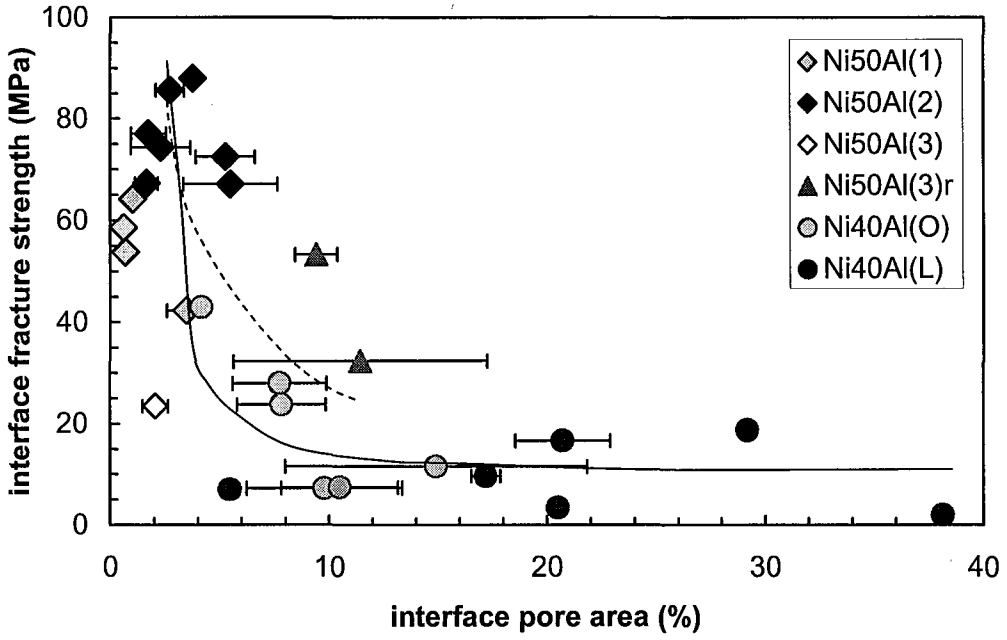

Figure 9: Relationship between interfacial strength and interface pore area. Data include oxidation times ranging from 26-100 hrs at 1000°C.